GEOPHYSICAL RESEARCH LETTERS, VOL. 23, NO. 7, PAGES 773-776, APRIL 1, 1996

The relationship between ELF-VHF waves and magnetic shear at the dayside magnetopause

Z. Zhu,[1] P. Song,[1] J. F. Drake,[2] C. T. Russell,[3] R. R. Anderson,[4]
D. A. Gurnett,[4] K. W. Ogilvie,[5] and R. J. Fitzenreiter[5]

Abstract. ELF-VLF waves within the current layer of the dayside magnetopause are studied using ISEE-1 data. The database consists of 272 current layer crossings at the dayside magnetopause from 1977 to 1979. For each crossing, the average intensity of ELF-VLF waves inside the current layer is obtained and the magnetic shear angle across the current layer is calculated from the magnetometer data. It is found that the wave amplitudes (both electric and magnetic fields), after normalization by the average magnetic field strength in the current layer, are proportional to the local magnetic shear angle, i.e. large magnetic shear corresponds to strong wave emission and vice versa. From the dispersion relation of the waves for different shear angles, the phase velocity of the waves increases with the magnetic shear and peaks around 700 Hz to 1 kHz. The dispersion curve of the waves is consistent with that of whistler modes.

Introduction

Enhancements of broadband ELF-VLF waves are often observed at the dayside magnetopause [*Gurnett et al.*, 1979; *Tsurutani et al.*, 1981, 1989; *Anderson et al.*, 1982; *LaBelle et al.*, 1987; *Song*, 1994]. The maximum frequency for waves is below 100 kHz for the electric component and below 1 kHz for the magnetic component. Figure 1 shows such an example. The ELF-VLF waves, magnetic fields and electron density measurements are from ISEE-1. In this example there are three well defined magnetopause current layer crossings, highlighted in Figure 1c by the shaded regions. Typically, broadband electromagnetic ELF-VLF waves are seen whenever there exists magnetic shear and these waves are usually strongest where the magnetic shear is greatest. Wave enhancement is most pronounced in the magnetic component of the wave (i.e. see Figure 1a).

The source of the electromagnetic ELF-VLF waves observed at the dayside magnetopause is yet not well understood. Instabilities, such as the lower hybrid drift instability (LHDI) [*Lemons and Gary*, 1977; *Gary and Eastman*, 1979; *Huba et al.*, 1981], and the electron anisotropy instability [e.g., *Kennel and Petschek*, 1969] may be possible candidates to generate the ELF-VLF waves. However, the frequency range associated with LHDI is usually below 10 Hz at the magnetopause which is much lower than the observed value.

Recent theory and numerical simulations have shown that whistler waves can be excited by the current driven instability associated with the gradient of the field-aligned current [*Drake et al.*, 1994]. A favorable condition for such an instability exists in the current layer of the Earth's magnetopause. At the magnetopause, the waves are unstable when there is a field-aligned current, or magnetic shear. In the dissipation region where reconnection is active, the waves are expected to be strong and these whistler type ELF-VLF waves may act as a detector for magnetic reconnection [*Drake et al.*, 1994].

Data Selection

Data from three instruments onboard ISEE-1 together with the solar wind data are used in this study. The University of Iowa plasma wave experiment [*Gurnett et al.*, 1978, 1979] provides 14 frequency channels of the magnetic field and 20 frequency channels of the electric field measurements. The channels are logarithmically spaced from 5.6 Hz to 10 kHz for the magnetic field and from 5.6 Hz to 311 kHz for the electric field. UCLA magnetometer [*Russell*, 1978] and the Vector Electron Spectrometer (VES) data [*Ogilvie et al.*, 1978] are used to identify the magnetopause crossing and the position of the current layer. Solar wind data from IMP-8 and/or ISEE-3 are used for references of the upstream conditions for future studies.

We restrict our attention to the ELF-VLF waves within the magnetopause current layer only. The magnetopause current layer is defined as the last rapid change in the field as the magnetospheric field is approached and can usually be well identified. Most of the crossings of the magnetopause current sheet last approximately 1 min with few over 10 min. We do not consider crossings that are less than 16 s, which is of the time resolution of the VES data. Neither do we consider crossings coincident with FTEs [*Russell and Elphic*, 1979] where the magnetic shear does not represent the magnetopause current layer alone. Cases are not included if there is no well defined magnetopause current layer crossing due to the fluctuations in the field and plasma parameters. We further restrict data to the dayside magnetopause, or within six hours of local noon.

[1] High Altitude Observatory, National Center for Atmospheric Research, Boulder, CO 80307.
[2] Institute for Plasma Research, University of Maryland, College Park, MD 20742.
[3] Institute of Geophysics and Planetary Physics, University of California, Los Angeles, CA 90095.
[4] Department of Physics and Astronomy, University of Iowa, Iowa City, IA 52242.
[5] NASA Goddard Space Flight Center, Greenbelt, MD 20771.

Paper number 96GL00591
0094-8534/96/96GL-00591$03.00

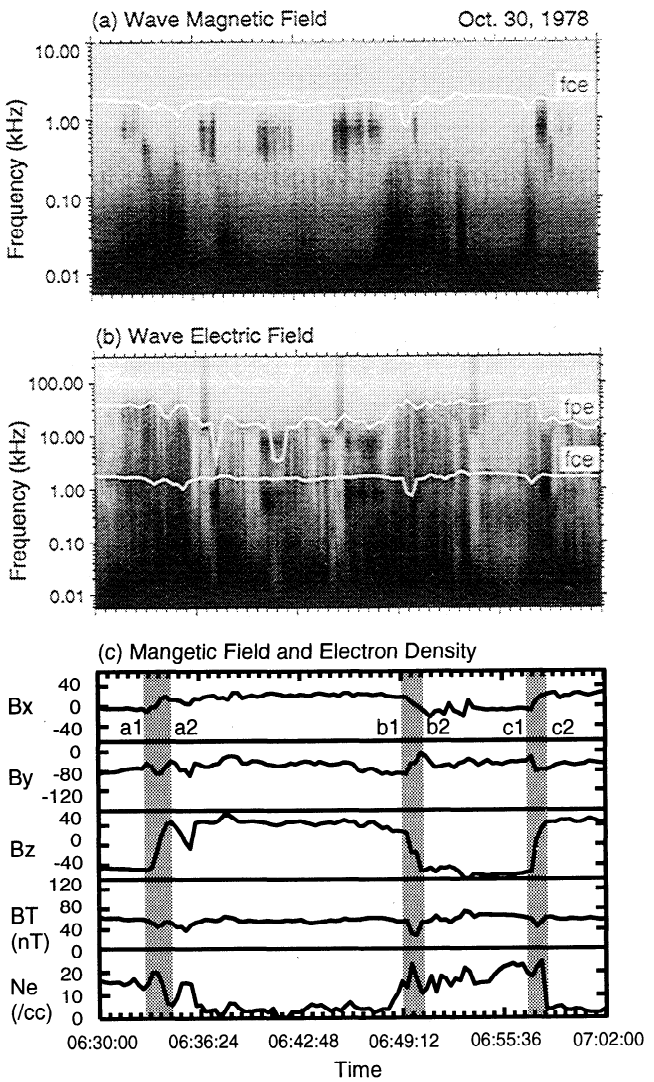

Figure 1. Diagram shows ELF-VLF waves associated with current layer crossings at the dayside magnetopause on Oct. 30, 1978. (a) and (b) are the wave magnetic and electric components measured by the Iowa plasma wave instrument. The darkness of the grey scale is proportional to logarithmic intensity. The magnetic field from UCLA magnetometer and the electron density from VES are shown in (c). Three current layer crossings are indicated as the shaded regions. White curves on (a) and (b) are the plasma frequency (f_{pe}) and the electron cyclotron frequency (f_{ce}).

In the example shown in Figure 1, which exhibits a strong ELF-VLF enhancement corresponding to each current layer crossing, the starting and ending times for the three crossings are marked as a1 and a2, b1 and b2, and c1 and c2, respectively. Note that there are ELF-VLF enhancements in other places in Figure 1 (e.g., at 06:35 UT and 06:38 UT). They represent partial crossings or local field and plasma fluctuations and are not of further interest here.

The final data set consists of 272 crossings from 130 passes from 1977 to 1979. Data cover the area at the dayside magnetopause between 33S to 45N of GSM latitude and between 6 to 18 hours of local time.

Magnetic Shear Dependence

Wave spectra are geometricly averaged over the period of each crossing. The averaged wave amplitude for each crossing is obtained by adding wave power in all the channels and taking square root of the power. The frequency range over which the averaged wave amplitude is derived involves 20 channels (5.6 Hz to 311 kHz) for the electric field and 14 channels (5.6 Hz to 10 kHz) for the magnetic field.

The shear angle θ is calculated using the magnetic field vectors ($\mathbf{B}_1$, $\mathbf{B}_2$) from the magnetometer at the starting and ending times for the crossing, a1 and a2, for example, using formula, $cos\theta = \mathbf{B}_1 \cdot \mathbf{B}_2/(|\mathbf{B}_1||\mathbf{B}_2|)$. The average value of the background magnetic field B_0 from the magnetometer is also obtained in the same period to normalize the wave fields. The normalized power is binned according to the corresponding magnetic shear angle. Each bin is 60° wide and overlaps 30° with neighboring bins on each side. The average (asterisk for the magnetic field and closed square for electric field) and its deviation (length of the vertical bar) for each bin are shown in Figure 2. The deviation of the mean for the wave magnetic field ranges from about 6% for large shear to 10% for small shear, and from 8% to 14% for wave electric field.

There is a clear correlation between the wave power and the shear angle. For large values of the shear, the amplitude of the waves is about double that for small shears. The solid and dashed lines are linear fits for the wave magnetic field and wave electric field, respectively. The values of the wave amplitudes at which the extrapolations of the two lines intersect the y axis at 0° shear angle give the noise level in this study assuming the nearly linear relationship. Here, the noise refers to waves whose origins are weakly associated with the field shear.

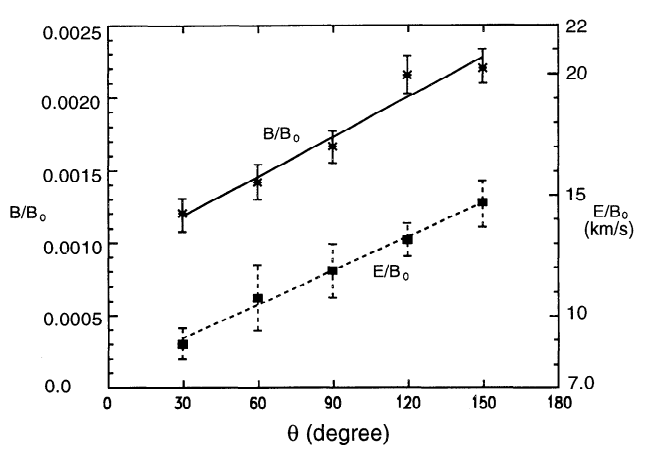

Figure 2. The amplitudes of the normalized wave magnetic field (asterisks) and wave electric field (closed squares) as functions of local magnetic shear angle. Vertical bars indicate the deviations of the means. Solid and dashed lines are the linear fits to the wave magnetic and electric data respectively.

Dispersion Relations

Wave amplitude at specific channel (frequency range) is derived by taking square root of the power of that channel. From the Faraday's law, the phase velocity is estimated from the wave amplitude $E(\omega)$ and $B(\omega)$, $v_{ph} = E(\omega)/B(\omega)$, where we have assumed that the electric perturbation is perpendicular to the propagation direction and that the measured electric and magnetic perturbations have the same proportionality as those of the waves. For electromagnetic modes (such as whistler modes propagating parallel to the background magnetic field), the assumptions usually hold. Since the ISEE-1 spin axis is nearly parallel to the dayside magnetospheric field, the perturbed fields are in the spin plane and our estimate of the phase velocity should be very accurate for whistler modes propagating along the magnetospheric field. The phase velocity as function of frequency gives the dispersion relation. Figure 3 show the dispersion relation for the five bins of different shears.

As we mentioned above, the wave spectra are averaged first over the period of each crossing in the time domain and then in the respective bin according to the local magnetic shear angle. The five curves in Figure 3 represent different magnetic shear levels as indicated. The phase velocity of the ELF-VLF waves peaks around 0.7~1 kHz and drops rapidly above 1 kHz. The typical magnetic field strength near the dayside magnetopause is 30 ~ 60 nT which translates to an electron cyclotron frequency of 0.8~1.7 kHz. Therefore, the phase velocity drop at high frequency is associated with electron cyclotron cutoff. Clear dispersion occurs from 70 Hz to 1 kHz. The phase velocity increases with frequency. The ascending tone is the characteristic of the whistler mode.

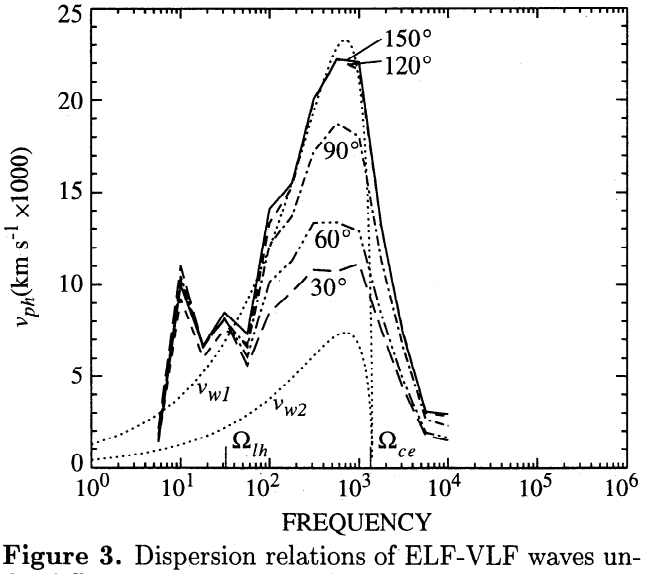

Figure 3. Dispersion relations of ELF-VLF waves under different magnetic shear levels. The two dotted lines (v_{w1} and v_{w2}) show the theoretical dispersion curves of whistler mode with a magnetic field strength of 50 nT and electron density of 1 cm^{-3} and 10 cm^{-3} respectively. Ω_{ce} and Ω_{lh} are the electron cyclotron frequency and the lower-hybrid frequency respectively.

To compare the dispersion curve from the measurements with that of the whistler mode, two dispersion curves (v_{w1} and v_{w2}) of whistler mode are plotted on Figure 3 (dotted lines) using the analytic formula $v_w = c\{1+\omega_{pe}^2/[\omega(\Omega_{ce}-\omega)]\}^{-1/2}$ where Ω_{ce} is the electron gyro-frequency, and ω_{pe} is the plasma frequency. The two curves are drawn with the same magnetic field strength of 50 nT but with different density values of 1 cm^{-3} for v_{w1} and 10 cm^{-3} for v_{w2}. We also include the electron cyclotron frequency (Ω_{ce}) and the lower-hybrid frequency ($\Omega_{lh} = \sqrt{\Omega_{ce}\Omega_{ci}}$) in Figure 3. From Figure 3, the dispersion curves of the whistler waves and the measured ELF-VLF waves match quite well for frequencies greater than the lower-hybrid frequency. The unrealistic value of density (1 cm^{-3}) for curve v_{w1} in Figure 3 indicates that the whistler dispersion equation may be altered at high shear.

Discussion

We have demonstrated, from a statistical point of view, a nearly linear relationship between the local magnetic shear angle and the amplitude of ELF-VLF waves in the current layer at the dayside magnetopause. We have also shown that the waves have a dispersion character consistent with whistler waves. The phase velocities of the waves are much greater than the Alfvén velocity at high shear.

A plausible interpretation of the data presented in Figures 2 and 3 is that there is a mixture of waves at the magnetopause. The dispersion curves in Figure 3 for the frequency below 60 Hz may due to the lower-hybrid waves [e.g, *Gary and Eastman*, 1979]. Because the lower-hybrid waves propagate nearly perpendicular to **B**, the assumptions used in our method to derive the dispersion relation do not apply. Therefore, the nearly non-dispersive curves in Figure 3 in the frequency range below 60 Hz do not have definitive meanings. Furthermore, the Alfvén waves, with a much smaller phase velocity, may well be buried in this portion of the dispersion curves. The dominant feature in Figure 3 is a whistler dispersion character with an amplitude which increases strongly with the shear. However, the unrealistic value of density used for the whistler dispersion curve to fit the measured dispersion curve may indicate some unknown mechanisms which alter the whistler characteristic at high shear.

These results have important implications for understanding magnetic reconnection at the magnetopause. In recent models the dynamics of whistlers has been established as a control mechanism for the rate of reconnection in collisionless plasma [*Mandt et al.*, 1994; *Drake et al.*, 1994; *Biskamp et al.*, 1995]. As a consequence, the generation of whistlers is intrinsically coupled to the reconnection process. Since the magnetic shear angle is a key parameter associated with magnetic reconnection, the strong dependence of the wave power on the field shear is consistent with the idea that reconnection is linked to the generation of ELF-VLF waves in the current layer. In other words, if magnetic reconnection indeed occurs over a large portion of the

Earth's magnetopause, it should occur most vigorously in regions of large magnetic shear, drive strong localized currents and produce strong ELF-VLF waves. Therefore, ELF-VLF waves may act as a signature of magnetic reconnection [*Drake et al.*, 1994] in addition to other evidence of reconnection from, for example, fast flows [*Paschmann et al.*, 1979; *Sonnerup et. al.*, 1981], and the plasma distribution function [e.g., *Gosling et al.*, 1990]. The present data, of course, provides only a plausible statistical link between the ULF-VLF waves and reconnection. There is as yet no direct observational evidence at the magnetopause linking magnetic reconnection with these waves.

The high phase velocity of whistler waves is critical to their importance in boosting the rate of magnetic reconnection in collisionless plasma. The intrinsic scale size of the dissipation region in collisionless plasma, where the frozen flux constraint is broken (allowing reconnection to occur), is the electron skin depth, $d_e = c/\omega_{pe}$ [*Vasyliunas*, 1975]. A straightforward Sweet-Parker analysis based on the Alfvén outflow velocity v_A yields the reconnection inflow rate $v_A d_e/L$, with L the characteristic system length. This is a very slow reconnection rate but is fortunately invalid. At scales of smaller than the ion inertial length $d_i = c/\omega_{pi}$ the electron and ion motion decouples [*Mandt et al.*, 1994] and whistlers rather than Alfvén waves govern the plasma dynamics. The maximum velocity of the whistler is of order $v_A(m_i/m_e)^{1/2}$, which is much higher than the Alfvén velocity. As a consequence, the dissipation region does not limit the reconnection rate. Rather the ion coupling to the outer MHD flows ultimately limits the rate to a velocity of order $v_A d_i/L$ [*Biskamp et al.*, 1995], which greatly exceeds previous estimates based on d_e. The rate increase requires the mediation of the high phase velocity whistler waves. Thus, the observation of these waves, as shown in Figure 3, is critical to the validation of these new ideas on collisionless reconnection.

Acknowledgments. Z. Zhu would like to thank the NCAR/HAO for the postdoctoral fellowship. Work at HAO was sponsored by the NSF and supported by NASA under research grant W-18582. Work at IPR was supported by NSF under research grant ATM93000988 and by NASA under NAGW-2079. Work at UCLA was supported by NASA under research grant NAGW-3948. We thank NSSDC for providing ISEE-1 data.

References

Anderson et al., Plasma waves near the magnetopause, *J. Geophys. Res., 87*, 2087, 1982.

Biskamp, D., E. Schwarz, J. F. Drake, Ion-controlled collisionless magnetic reconnection, *Phys. Rev. Lett. to appear*, 1995.

Drake, J. F., R. G. Kleva, and M. E. Mandt, Structure of thin current layers: Implications for magnetic reconnection, *Phys. Rew. Lett., 73*, 1251, 1994.

Gary, S. P., and T. E. Eastman, The lower hybrid drift instability at the magnetopause, *J. Geophys. Res., 84*, 7378, 1979.

Gosling et al., The electron edge of the low latitude boundary layer during accelerated flow events, *Geophys. Res. Lett., 17*, 1883, 1990.

Gurnett, D. A., F. L. Scarf, R. W. Fredricks, and E. J. Smith, The ISEE 1 and ISEE 2 plasma wave investigation, *IEEE Trans. Geosci. Electron., GE-16*, 225, 1978.

Gurnett et al., Plasma wave turbulence at the magnetopause: Observations from ISEE 1 and 2, *J. Geophys. Res., 84*, 7043, 1979.

Huba, J. D., N. T. Gladd, and J. F. Drake, On the role of the lower hybrid drift instability in substorm dynamics, *J. Geophys. Res., 86*, 5881, 1981.

Kennel, C. F., and H. E. Petschek, Limit on stably trapped particle fluxes, *J. Geophys. Res., 71*, 1, 1966.

LaBelle et al., AMPTE IRM observations of waves associated with flux transfer events in the magnetosphere, *J. Geophys. Res., 92*, 5827, 1987.

Lemons, D. S., and S. P. Gary, Electromagnetic effects on the modified two-stream instability, *J. Geophys. Res., 82*, 2337, 1977.

Mandt, M. E., R. E. Denton, and J. F. Drake, Transition to whistler mediated magnetic reconnection, *Geophys. Res. Lett., 21*, 73, 1994.

Ogilvie, K. W., J. D. Scudder and H. Doong, The electron spectrometer on ISEE 1, *IEEE Trans. Geosci. Electron., GE-16*, 261, 1978.

Paschmann et al., Plasma acceleration at the earth's magnetopause: Evidence for reconnection, *Nature, 282*, 243-246, 1979.

Russell, C. T., The ISEE 1 and 2 fluxgate magnetometers, *IEEE Trans. Geosci. Electron., GE-16*, 239, 1978.

Russell, C. T., R. C. Elphic, ISEE observations of flux transfer events at the dayside magnetopause, *Geophys. Res. Lett., 6*, 33, 1979.

Song, P., Observations of waves at the dayside magnetopause, in *Solar Wind Sources of Magnetospheric Ultra-Low-Frequency Waves*, Geophys. Monogr., vol 81, edited by M. J. Engebretson, K. Takahashi, and M. Scholer, AGU, Washington, D.C., 1994.

Sonnerup et al., Evidence for magnetic field reconnection at the earth's magnetopause, *J. Geophys. Res., 86*, 10,049, 1981.

Tsurutani et al., A statistical study of ELF-VLF plasma waves at the magnetopause, *J. Geophys. Res., 94*, 1270, 1989.

Tsurutani et al., Wave-particle interactions at the magnetopause: Contributions to the dayside aurora, *Geophys. Res. Lett., 8*, 183, 1981.

Vasyliunas, V. M., Theoretical models of magnetic field line merging, *Rev. Geophys., 13*, 303, 1975.

(received November 6, 1995; revised February 8, 1996; accepted February 12, 1996.)